Theoretical and Experimental Study of the Gas-Phase Reactions of PF_n^+ ($n = 1, 2$) Ions with n-Bases. A Novel Route to Phosphorus Ions Present in Interstellar Clouds§

Antonello Filippi,† Giorgio Occhiucci,‡ and Maurizio Speranza*,†

Facoltà di Farmacia, Dipartimento di Studi di Chimica e Tecnologia delle Sostanze Biologicamente Attive, Università di Roma "La Sapienza", 00185 Rome, Italy, and Istituto di Chimica Nucleare e Servizio FTMS del CNR, Area della Ricerca del CNR, 00016 Monterotondo Stazione, Rome, Italy.

Received November 20, 1996⊗

The reactivity of PF_n^+ ($n = 1, 2$) cations toward n-type bases, such as H_2O, CH_3OH, and NH_3, has been investigated using Fourier-transform ion cyclotron resonance (FT-ICR) mass spectrometry. Both phosphorus ions attack the n-center of the selected bases, yielding the corresponding excited onium intermediates, which undergo extensive prototropic rearrangements before fragmenting with formal losses of H and HF (with H_2O and NH_3) or HF, CH_3, and CH_3F (with CH_3OH). Ab initio molecular orbital calculations at the G2 level of theory have been used to study the structures, the relative stability, and the proton loss energies of the ionic species involved in these reactions. The G2 $[PF, H_2O]^+$ and $[PF, NH_3]^+$ potential energy profiles conform well with the FT-ICR reaction kinetics. Unequivocal assignment of the structure and the multiplicity of several ionic species obtained from the title reactions and potentially involved in the formation of phosphorus-containing molecules in outer space, i.e. $(PO)H^+$, $(FPO)H^+$, $(PNH)H^+$, and $(FPNH)H^+$, is allowed by a comparison of their G2-calculated proton loss energies with the experimental protonation enthalpies, measured in the FT-ICR instrument with the bracketing technique. The emerging picture has been compared with previous theoretical data concerning strictly related species wherein the phosphorus atom is replaced by nitrogen.

Introduction

In the last few years, gas-phase chemistry of phosphorus has enjoyed a renewed interest after detection of various phosphorus-containing molecules in planets' atmospheres[1] and in different nebulae.[2] Because the most likely routes to formation of phosphorus-containing molecules in space[3] are ionic, a number of experimental[4] and theoretical[5] studies on the nature and the behavior of isolated phosphorus ions have been carried out. Experimental kinetic investigations[4] using ion-cyclotron resonance and selected ion flow tube techniques pointed to facile insertion of PH_n^+ ($n = 0-4$) into the covalent bonds of simple molecules, such as NH_3, CH_3NH_2, CH_3CCH, etc., as a pathway to phosphorus species, such as PN and PC, detected in sidereal media.[2] In the same studies, conceivable ionic paths to other potential phosphorus interstellar species, such as PYH_n (Y = O ($n = 0-2$), N ($n = 1, 2$), C ($n = 1-4$), S ($n = 0-2$)), have been suggested as well. However, after these kinetic investigations, several questions still remained unanswered, such as the thermochemistry and the detailed mechanism for the insertion of phosphorus ions into covalent bonds of the neutrals. It was also desirable to have information on the structure and electronic configuration of the ionic products arising from these reactions.

A number of theoretical studies have addressed the above questions.[5−11] The proton affinities (PA's) of some PYH_n species, including those with Y = O ($n = 0, 1$),[6,7] Y = N ($n = 0-3$),[6,8] Y = C ($n = 1$),[6] and Y = S ($n = 0, 1$),[6,9] have been estimated at different ab initio theoretical levels. Theoretical studies of the reactions of ground-state (^3P) and excited (^1D)

† Università di Roma.

‡ CNR.

§ Dedicated to Professor Fulvio Cacace on the occasion of his 65th birthday.

⊗ Abstract published in *Advance ACS Abstracts,* July 15, 1997.

(1) Ridgeway, S. T.; Wallace, L.; Smith, G. R. *Astrophys. J.* **1976**, *207*, 1002.

(2) (a) Turner, B. E.; Bally, J. *Astrophys. J. Lett.* **1987**, *321*, L75. (b) Ziurys, L. M. *Astrophys. J. Lett.* **1987**, *321*, L81. (c) Guelin, M.; Cernicharo, J.; Paubert, G.; Turner, B. E. *Astron. Astrophys.* **1990**, *230*, L9.

(3) Duley, W. W.; Williams, D. A. *Interstellar Chemistry*; Academic Press: New York, 1984.

(4) (a) Thorne, L. R.; Anicich, V. G.; Huntress, W. T. *Chem. Phys. Lett.* **1983**, *98*, 162. (b) Thorne, L. R.; Anicich, V. G.; Prasad, S. S.; Huntress, W. T. *Astrophys. J.* **1984**, *280*, 139. (c) Smith, D.; McIntosh, B. J.; Adams, N. G. *J. Chem. Phys.* **1989**, *90*, 6213. (d) Adams, N. G.; McIntosh, B. J.; Smith, D. *Astron. Astrophys.* **1990**, *232*, 443.

(5) (a) Trinquier, G. *J. Am. Chem. Soc.* **1982**, *104*, 6969. (b) Gonbeau, D.; Pfister-Guillouzo, G.; Barrans, J. *Can. J.. Chem.* **1983**, *61*, 1371. (c) Ha, T. K.; Nguyen, M. T.; Ruelle, P. *Chem. Phys.* **1984**, *87*, 23. (d) Nguyen, M. T.; McGinn, M. A.; Hegarty, A. F. *J. Am. Chem. Soc.* **1985**, *107*, 8029. (e) Allen, T. L.; Scheiner, A. C.; Yanaguchi, Y.; Schaefer, H. F., III. *Chem. Phys. Lett.* **1985**, *121*, 154. (f) Ito, K.; Nagase, S. *Chem. Phys. Lett.* **1986**, *126*, 531. (g) Berkowitz, J.; Curtiss, L. A.; Gibson, S. T.; Greene, J. P.; Hillhouse, G. L.; Pople, J. A. *J. Chem. Phys.* **1986**, *84*, 375. (h) Lohr, L. L.; Boehm, R. C. *J. Phys. Chem.* **1987**, *91*, 3207. (i) Bruna, P. J.; Grein, F. *J. Phys. B: At. Mol. Phys.* **1987**, *20*, 5967. (j) Nguyen, M. T.; Hegarty, A. F.; Ha, T. K.; Brint, P. *Chem. Phys. Lett.* **1985**, *98*, 447. (k) Bachrach, S. M. *J. Comput. Chem.* **1989**, *10*, 392. (l) Ahlrichs, R.; Bar, M.; Plitt, H. S.; Schnockel, H. *Chem. Phys. Lett.* **1989**, *161*, 179.

(6) Maclagan, R. G. A. R. *J. Phys. Chem.* **1990**, *94*, 3373.

(7) Redondo, P.; Largo, A.; Barrientos, C.; Ugalde, J. M. *J. Phys. Chem.* **1991**, *95*, 4318.

(8) (a) Glaser, R.; Horan, C. J.; Choy, G. S. C.; Harris, B. L. *J. Phys. Chem.* **1992**, *96*, 3689. (b) Glaser, R.; Horan, C. J.; Haney, P. E. *J. Phys. Chem.* **1993**, *97*, 1835.

(9) Lopez, X.; Ugalde, J. M.; Barrientos, C.; Largo, A.; Redondo, P. *J. Phys. Chem.* **1993**, *97*, 1521.

(10) (a) Largo, A.; Flores, J. R.; Barrientos, C.; Ugalde, J. M. *J. Phys. Chem.* **1991**, *95*, 5443. (b) Largo, A.; Flores, J. R.; Barrientos, C.; Ugalde, J. M. *J. Phys. Chem.* **1991**, *95*, 6553. (c) Largo, A.; Flores, J. R.; Barrientos, C.; Ugalde, J. M. *J. Phys. Chem.* **1991**, *95*, 170. (d) Largo, A.; Barrientos, C. *J. Phys. Chem.* **1991**, *95*, 9864.

(11) (a) Esseffar, M.; Luna, A.; Mo, O.; Yanez, M. *J. Phys. Chem.* **1993**, *97*, 6607. (b) Esseffar, M.; Luna, A.; Mo, O.; Yanez, M. *Chem. Phys. Lett.* **1993**, *209*, 557. (c) Largo, A.; Barrientos, C.; Lopez, X.; Ugalde, J. M. *J. Phys. Chem.* **1994**, *98*, 3985. (d) Esseffar, M.; Luna, A.; Mo, O.; Yanez, M. *J. Phys. Chem.* **1994**, *98*, 8679. (e) Esseffar, M.; Luna, A.; Mo, O.; Yanez, M. *Chem. Phys. Lett.* **1994**, *223*, 240. (f) Cruz, E. M.; Lopez, X.; Ugalde, J. M.; Cossio, F. P. *J. Phys. Chem.* **1995**, *99*, 12170.

S0020-1669(96)01394-8 CCC: $14.00

P^+ ions with a variety of molecules relatively abundant in the outer space have been reported as well,[10,11] revealing new conceivable routes to still undetected phosphorus species in the outer space. Nevertheless, the very limited availability of experimental data in this area does not allow us to evaluate the adequacy of the theoretical levels employed. In fact, phosphorus-containing ions offer paradigmatic examples where both structures and relative energies are very sensitive to the level of theory used to describe them. The problem may be particularly severe for open-shell systems, such as $[H, P, O]^+$ [4d,6] and $[H_2, P, N]^+$.[11a]

This paper represents a contribution to the characterization of oxygen- and nitrogen-containing phosphorus ions, based upon Fourier-transform ion cyclotron resonance (FT-ICR) kinetic measurements and *ab initio* theroretical calculations. The ions investigated arise from the gas-phase attack on H_2O, CH_3OH, and NH_3 by the PF_n^+ ($n = 1, 2$) ions obtained from electron bombardment of PF_3. These reactions represent viable routes to a variety of oxygen- and nitrogen-containing phosphorus ions, including $[H, P, O]^+$ and $[H_2, P, N]^+$, whose reactivity and stability features can be determined from the corresponding efficiencies of reactions with selected substrates.

Experimental Section

Materials. PF_3 was a research grade gas from UCAR Specialty Gases NV, with a minimum purity of 99.6 mol %. Before use, the gas was further purified by passage through an anhydrous $KF-SiO_2$-packed column kept at 0 °C. The other chemicals used as substrates or as reference compounds in the FT-ICR bracketing experiments, obtained from commercial sources in research grade purity, were degassed by several freeze−pump−thaw cycles at 77 K before use. In the case of gaseous reagents, purification by preliminary distillation in a vacuum line was utilized.

Procedure. The experiments were carried out in the dual cell of a 3-T Extrel FTMS 2001 mass spectrometer, equipped with an Odyssey data station and an FTMS Autoprobe. This instrumental configuration is particularly well suited for our purposes because the neutral precursors of the desired phosphorus ions, e.g. PF_3, are physically separated from the neutral target molecule. Hence, any interference from neutral products conceivably arising from thermal reactions between reactive neutrals can be safely excluded. Thus, PF_3 (sometimes mixed with other neutral gases) was introduced into the source chamber of the instrument at pressures around 1×10^{-6} Torr and bombarded with 70 eV electrons. The ionic fragments were injected into the analyzer chamber containing exclusively the neutral of interest at pressures around 1×10^{-7} Torr. After sequential isolation of the ion of interest by the SWIFT procedure, argon was pulsed in the analyzer by a pulsed magnetic valve in order to reach pressures up to 5×10^{-5} Torr, albeit for a short time (<5 ms). After 0.5 s of pumping, the Ar partial pressure dropped again to zero. During this time, the translationally and vibrationally excited reactant ions were efficiently quenched by collisions with the Ar atoms and partly converted into products by collision with the more diluted substrate. Once thermalized, the ion of interest was isolated again by the SWIFT procedure and its progeny analyzed after various delay times. The decrease of the logarithm of the relative abundance of the starting ionic reactant with the reaction time was observed to be linear, as required for thermally equilibrated reactants. The concentration of the neutral substrate in the analyzer chamber was determined from the pressure measured by the ionization gauge located at the high-vacuum pumping line of the FT-ICR cell housing. The ionization gauge was calibrated with the reference reaction $CH_4^+ + CH_4 \rightarrow CH_5^+ + CH_3$, using as its rate constant the well-established value of 1.13×10^{-9} cm^3 molecule^{-1} s^{-1}.[12] Subsequently, the correction factor needed for other compounds was estimated with a method based on an indicated linear dependence of the response of the ionization gauge on the polarizability of the neutral reagent in question.[13]

Computational Details. The ab initio calculations were carried out using an RISC/6000 version of the Gaussian 94 set of programs.[14] The geometries of the investigated species were optimized at the HF/6-31G* and MP2/6-31G* levels of theory (the latter was used without frozen core orbitals and will be denoted as MP2(FULL)/6-31G*), without imposing any symmetry constraints, and their harmonic vibrational frequencies were computed at both calculation levels. Approximate QCISD(T)/6-311+G(3df,2p) energies were calculated at the MP2(FULL)/6-31G* optimized geometries using the GAUSSIAN-2 (G2) procedure[15] implemented as a standard routine in Gaussian 94. This computational method is widely recognized as being able to reproduce or predict unknown thermochemical data (atomization energies, ionization potentials, electron affinities, and proton affinities) for compounds containing first- and second-row elements with a target accuracy of ±2 kcal mol^{-1}. Within the G2 theory, the zero-point vibrational energies (ZPEs) of all the investigated species are obtained by the HF/6-31G* frequencies scaled by 0.8929. The 0 K total energies of the investigated species, E_0, can be therefore estimated from the relevant G2 and ZPE values. The corresponding 298.15 K total energies are obtained by adding to the E_0 values the translational ($^3/_2RT$), rotational (RT or $^3/_2RT$ for linear and nonlinear species, respectively), and vibrational contributions. The latter factors are calculated by standard statistical mechanics[16] formulas using the HF/6-31G* vibrational frequencies scaled as required by the G2 methodology. Finally, the 298.15 K total energies are corrected to enthalpies, H_{298}, by assuming ideal gas behavior and adding the proper ΔnRT contribution. The corresponding 298.15 K free energies, G_{298}, were obtained by adding to H_{298} the appropriate $-TS_{298}$ terms.

Results and Discussion

The Ionic Reactants. Ab initio calculations[17] agree with experimental evidence[18] in assigning to the PF^+ ground state the $^2\Pi$ configuration. The calculated bond length of $PF^+(^2\Pi)$ (1.519 Å) is in reasonable agreement with the experimental value (1.500 Å).[18] While the $^2\Pi$ ground state of PF^+ is bound by ca. 84 kcal mol^{-1}, its $^4\Sigma^-$ excited state is calculated to be unbound relative to the separated atoms. Bonding in $PF^+(^2\Pi)$ is predominantly ionic with a great deal of the positive charge on the P atom and some π-donation from F to P.[17]

Different ab initio theoretical approaches converge in assigning the $^1A_1$ configuration to ground state PF_2^+.[17,19] The $PF_2^+(^1A_1)$ bond length is 1.525 Å, and the F−P−F bond angle is 102.3°.[19] Theoretical predictions are confirmed by the coincidence between the computed (8.803 eV) and the experimental values (8.847 ± 0.01 eV) of the adiabatic ionization energy of PF_2 for the process $PF_2(^2B_1) \rightarrow PF_2^+(^1A_1) + e^-$.[20] The $^1A_1$ ground state of PF_2^+ is bound by ca. 100 kcal mol^{-1} relative to

(12) (a) Olmstead, W. N.; Brauman, J. I. *J. Am. Chem. Soc.* **1977**, *99*, 4219. (b) Ikezoe, Y.; Matsuoka, S.; Takebe, M.; Viggiano, A. A. *Gas-Phase Ion-Molecule Reaction Rate Constants Through 1986*; Maruzen: Tokyo, 1987.

(13) Bartmess, J. E.; Georgiadis, R. M. *Vacuum* **1983**, *33*, 149.

(14) Frish, M. J.; Trucks, G. W.; Schlegel, H. B.; Gill, P. M. W.; Johnson, B. G.; Robb, M. A.; Cheeseman, J. R.; Keith, T. A.; Petersson, G. A.; Montgomery, J. A.; Raghavachari, K.; Al-Laham, M. A.; Zakrzewski, V. G.; Ortiz, J. V.; Foresman, J. B.; Cioslowski, J.; Stefanov, B. B.; Nanayakkara, A.; Challacombe, M.; Peng, C. Y.; Ayala, P. Y.; Chen, W.; Wong, M. W.; Andres, J. L.; Repogle, E. S.; Gomperts, R.; Martin, R. L.; Fox, D. J.; Binkley, J. S.; Defrees, D. J.; Baker, J.; Stewart, J. P.; Head-Gordon, M.; Gonzales, C.; Pople, J. A. *Gaussian 94*, Revision C.2, Gaussian, Inc.: Pittsburgh, PA, 1995.

(15) Curtiss, L. A.; Raghavachari, K.; Trucks, G. W.; Pople, J. A. *J. Chem. Phys.* **1991**, *94*, 7221.

(16) McQuarrie, D. *Statistical Mechanics*; Harper and Row: New York, 1976.

(17) Harrison, J. F. *J. Am. Chem. Soc.* **1981**, *103*, 7406.

(18) (a) Narasimahan, N. A. *Can. J. Phys.* **1957**, *35*, 901. (b) Douglas, A. E.; Franckowiak, M. *Can. J. Phys.* **1962**, *40*, 832.

(19) Latifzadeh, L.; Balasubramanian, K. *Chem. Phys. Lett.* **1994**, *228*, 463.

(20) (a) Berkowitz, J.; Greene, J. P.; Foropoulos, J., Jr.; Neskovic, O. M. *J. Chem. Phys.* **1984**, *81*, 6166. (b) Butcher, V.; Dyke, J. M.; Lewis, A. E.; Morris, A.; Rihda, R. A. *J. Chem. Soc., Faraday Trans.* **1988**, *284*, 299.

Scheme 1

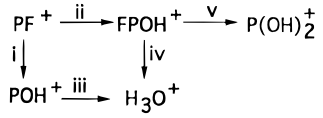

Scheme 2

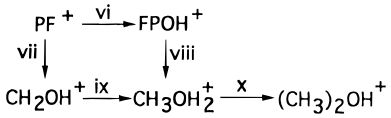

Scheme 3

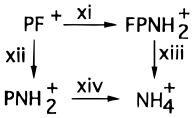

Scheme 4

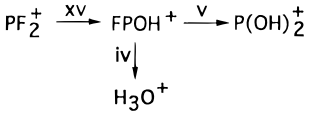

Scheme 5

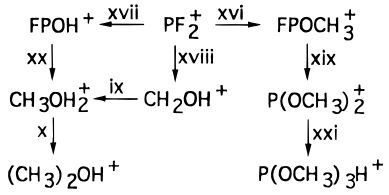

Scheme 6

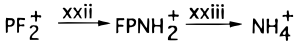

the separated $PF^+(^2\Pi)$ and $F(^2P)$ moieties and lies 89.9 kcal mol^{-1} lower in energy relative to its $^3B_1$ first excited state.[20] As for $PF^+(^2\Pi)$, the bonds of $PF_2^+(^1A_1)$ have a pronounced ionic character, with the positive charge mostly located on the P atom and some π-donation from F to P.[20]

In view of the substantial energy gaps between the ground states of PF_n^+ ($n = 1, 2$) and their first excited states, electron impact on PF_3 in the FT-ICR source is expected to generate ground-state $PF^+(^2\Pi)$ and $PF_2^+(^1A_1)$. Accordingly, the time dependence of the logarithm of the relative abundance of the PF_n^+ ($n = 1, 2$) reactants in their reactions with the selected n-bases is linear within the the entire time range covered (up to 10 s), thus indicating that the incursion of excited PF_n^+ ($n = 1, 2$) is negligible.

Reaction Mechanisms. The FT-ICR ion patterns from the attack of PF^+ ions on water, methanol, and ammonia are reported in Schemes 1−3, respectively. Those from reaction of PF_2^+ ions with the same neutrals are given in Schemes 4−6. All steps of Schemes 1−6 involve a reactive collision between the neutral substrate and the corresponding ion, whose actual structure remains undefined. In almost all cases, formation of the ionic products is accompanied by release of neutral fragments, which cannot be detected with the experimental method used. Thus, no structural significance must be attached to the formulas of the reactants and products of the ion−molecule reactions reported below, unless otherwise specified.

The reaction networks of Schemes 1−6 were determined by analysis of the dependence of the corresponding ion abundances on the reaction time. A typical case is illustrated in Figure 1, concerning the reaction of PF^+ with H_2O.

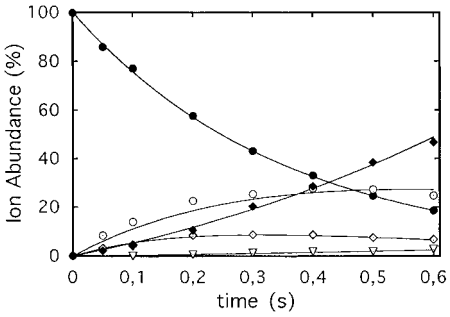

Figure 1. Time dependence of ion abundances following attack of PF^+ on H_2O (2.3×10^{-7} Torr): PF^+ (full circles); $[H, P, O]^+$ (open circles); $[F, H, P, O]^+$ (open diamonds); $[H_2, P, O_2]^+$ (triangles); H_3O^+ (full diamonds).

Best fitting of the experimental points is represented by the reported solid lines, which obey the reaction network of Scheme 1 with the following first-order rate constants (in s^{-1}): 2.0 (step i); 0.8 (step ii); 2.5 (step iii); 3.2 (step iv); 0.7 (step v). Further support for the specific reaction sequences of Schemes 1−6 arises from multiple resonance experiments, which allow isolation of the ion of interest (e.g., POH^+) by applying appropriate frequency windows to remove all the undesired ions from the cell and analysis of its progeny (i.e., H_3O^+) after a suitable reaction time. The first-order rate constants of the individual steps of Schemes 1−6, obtained from the best fitting procedure, were used to derive the corresponding second-order values (k_{obs}), reported in Tables 1 (for PF^+) and 2 (for PF_2^+). The relevant reaction efficiencies are calculated from the ratio between the experimental k_{obs} and the collision rate constants (k_{coll}), estimated according to the trajectory calculation method.[21] Coincidence, within the experimental uncertainty (ca. 20%), of the efficiency values for the same reactions measured in different systems (e.g., steps iv and v of Tables 1 and 2) is somewhat reassuring regarding the soundness of the kinetic methodology adopted.

Analysis of Table 2 indicates that PF_2^+ attacks the selected substrates with an overall efficiency increasing with the basicity of the nucleophile, namely in the order H_2O (0.05) < CH_3OH (0.19) < NH_3 (0.20). The behavior of PF_2^+ fully conforms to that of other closed-shell fluorinated cations, such as SiF_3^+,[22] CF_3^+,[23] NF_2^+,[24] etc., which readily eliminate one HF molecule (or more) from their encounter complex with H_2O and NH_3 (steps xv and xxii in Table 2). With methanol, HF elimination (step xvi in Table 2) is accompanied both by the more efficient release of the CH_3F molecule to give $FPOH^+$ (step xvii in Table 2) and by a slow hydride transfer process to yield CH_2OH^+ (step xviii in Table 2).[22,23] While $FPOH^+$ rapidly protonates the bulk methanol (eff = 0.85; step xx in Table 2), the $FPOCH_3^+$ ion further adds to the substrate to yield $P(OCH_3)_2^+$ and eventually $P(OCH_3)_3H^+$ (steps xix → xxi in Table 2).[23a] The mechanistic details of this sequence were inferred by using labeled methanols CH_3OH (with **H** = D and **O** = ^{16}O or with

(21) Su, T.; Chesnavich, W. J. *J. Chem. Phys.* **1982**, *76*, 5183.
(22) (a) Grandinetti, F.; Occhiucci, G.; Ursini, O.; de Petris, G.; Speranza, M. *Int. J. Mass Spectrom. Ion Processes* **1993**, *124*, 21. (b) Crestoni, M. E.; Speranza, M. *Int. J. Mass Spectrom. Ion Processes* **1994**, *130*, 143.
(23) (a) Grandinetti, F.; Occhiucci, G.; Crestoni, M. E.; Fornarini, S.; Speranza, M. *Int. J. Mass Spectrom. Ion Processes* **1993**, *127*, 123. (b) Grandinetti, F.; Occhiucci, G.; Crestoni, M. E.; Fornarini, S.; Speranza, M. *Int. J. Mass Spectrom. Ion Processes* **1993**, *127*, 137.
(24) (a) Aschi, M.; Grandinetti, F.; Pepi, F. *Int. J. Mass Spectrom. Ion Processes* **1994**, *130*, 117. (b) Aschi, M.; Cacace, F.; Grandinetti, F.; Pepi, F. *J. Phys. Chem.* **1994**, *98*, 2713.

Table 1. Product Patterns and Rate Constants (k_{obs}) of the Reactions of $PF^+(^2\Pi)$ Ions with Selected Substrates

no.	reaction	k_{obs}[a] (10^{10} cm^3 molecule^{-1} s^{-1})	k_{coll}[b] (10^{10} cm^3 molecule^{-1} s^{-1})	efficiency
i	$PF^+ + H_2O \rightarrow POH^+ + HF$	2.7	24.6	0.12
ii	$PF^+ + H_2O \rightarrow FPOH^+ + H$	1.1	24.6	0.05
iii	$POH^+ + H_2O \rightarrow H_3O^+ + PO$	3.4	24.6	0.14
iv	$FPOH^+ + H_2O \rightarrow H_3O^+ + FPO$	4.4	23.7	0.18
v	$FPOH^+ + H_2O \rightarrow P(OH)_2^+ + HF$	1.1	23.7	0.05
vi	$PF^+ + CH_3OH \rightarrow FPOH^+ + CH_3$	6.1	21.7	0.28
vii	$PF^+ + CH_3OH \rightarrow CH_2OH^+ + PHF$	3.1	21.7	0.14
viii	$FPOH^+ + CH_3OH \rightarrow CH_3OH_2^+ + FPO$	14.4	19.8	0.73
ix	$CH_2OH^+ + CH_3OH \rightarrow CH_3OH_2^+ + CH_2O$	19.2	23.2	0.83
x	$CH_3OH_2^+ + CH_3OH \rightarrow (CH_3)_2OH^+ + H_2O$	1.7	22.8	0.07
xi	$PF^+ + NH_3 \rightarrow FPNH_2^+ + H$	6.4	22.1	0.29
xii	$PF^+ + NH_3 \rightarrow PNH_2^+ + HF$	1.4	22.1	0.06
xiii	$FPNH_2^+ + NH_3 \rightarrow NH_4^+ + FPNH$	15.8	21.4	0.74
xiv	$PNH_2^+ + NH_3 \rightarrow NH_4^+ + PNH$	13.8	22.3	0.62

[a] Uncertainty range ca. 20%. [b] Estimated according to the trajectory calculation method.[21]

Table 2. Product Patterns and Rate Constants (k_{obs}) of the Reactions of $PF_2^+(^1A_1)$ Ions with Selected Substrates

no.	reaction	k_{obs}[a] (10^{10} cm^3 molecule^{-1} s^{-1})	k_{coll}[b] (10^{10} cm^3 molecule^{-1} s^{-1})	efficiency
xv	$PF_2^+ + H_2O \rightarrow FPOH^+ + HF$	1.1	23.6	0.05
iv	$FPOH^+ + H_2O \rightarrow H_3O^+ + FPO$	3.9	23.7	0.16
v	$FPOH^+ + H_2O \rightarrow P(OH)_2^+ + HF$	0.9	23.7	0.04
xvi	$PF_2^+ + CH_3OH \rightarrow FPOCH_3^+ + HF$	1.0	19.7	0.05
xvii	$PF_2^+ + CH_3OH \rightarrow FPOH^+ + CH_3F$	2.6	19.7	0.13
xviii	$PF_2^+ + CH_3OH \rightarrow CH_2OH^+ + PHF_2$	0.2	19.7	0.01
xix	$FPOCH_3^+ + CH_3OH \rightarrow P(OCH_3)_2^+ + HF$	1.6	19.2	0.08
xx	$FPOH^+ + CH_3OH \rightarrow CH_3OH_2^+ + FPO$	16.8	19.8	0.85
xxi	$P(OCH_3)_2^+ + CH_3OH \rightarrow P(OCH_3)_3H^+$	1.2	12.6	0.09
ix	$CH_2OH^+ + CH_3OH \rightarrow CH_3OH_2^+ + CH_2O$	18.8	23.2	0.81
x	$CH_3OH_2^+ + CH_3OH \rightarrow (CH_3)_2OH^+ + H_2O$	1.3	22.8	0.06
xxii	$PF_2^+ + NH_3 \rightarrow FPNH_2^+ + HF$	4.3	21.3	0.20
xiii	$FPNH_2^+ + NH_3 \rightarrow NH_4^+ + FPNH$	15.8	21.4	0.74

[a] Uncertainty range ca. 20%. [b] Estimated according to the trajectory calculation method.[21]

H = H and **O** = ^{18}O) as substrates. Thus, attack of $FPOCH_3^+$ on C**H**$_3$**O**H leads to both $(CH_3O)P(\mathbf{O}C\mathbf{H}_3)^+$ (with elimination of HF; step xix in Table 2) and $FP\mathbf{O}C\mathbf{H}_3^+$ (with release of CH_3OH) with comparably low efficiencies (0.08 vs 0.09).[22b] No formation of C**H**$_3$**O**(H)CH_3^+ was observed. These results, coupled with the slow formation of $P(OH)_2^+$ from attack of H_2O on $FPOH^+$ (step v in Tables 1 and 2), point to the distinct selectivity of oxygenated bases for the phosphorus center of $FPOH^+$ and $FPOCH_3^+$ to give the corresponding complexes, wherein hydrogen migration over their n-centers probably involves substantial activation barriers. No HF elimination is observed from the attack of $FPOC\mathbf{H}_3^+$ (with **H** = H or D) on NH_3, which gives rise exclusively to C**H**$_3NH_3^+$. This behavior denotes the tendency of ammonia to attack the C center, rather than the P one, in contrast with the behavior of oxygenated bases.

The behavior of PF^+ toward the same substrates is somewhat different, since the overall reaction efficiency does not follow the basicity order of the selected nucleophiles but rather increases in the order H_2O (0.17) < NH_3 (0.35) < CH_3OH (0.42) (Table 1). Elimination of HF from the relevant encounter complexes generally competes with the release of an H atom (steps ii and xi in Table 1). With methanol, HF elimination is not observed, the major fragmentation routes being characterized by the release of either CH_3 or PHF (steps vi and vii in Table 1).

Some insights into the energetics and the kinetics of competing paths i and ii of Scheme 1 and paths xi and xii of Scheme 3 have been obtained by analysis of the relevant $[PF, H_2O]^+$ and $[PF, NH_3]^+$ potential energy surfaces (PES's).

Concerning the $[PF, H_2O]^+$ PES, several critical structures have been located along the reaction coordinate that connects the $PF^+(^2\Pi)$ and H_2O reactants to their products. Their optimized geometries, calculated at the MP2(FULL)/6-31G* level of theory, are shown in Figure 2. The relevant data for the evaluation of the corresponding G2 energies are given in Table 3. A schematic view of the two-dimensional $[PF, H_2O]^+$ PES is reported in Figure 3.

The structure of $F-PH-OH^+$ (**2**) represents the global minimum of the $[PF, H_2O]^+$ PES. It is connected to the 3.6 kcal mol^{-1} less stable isomer $FP-OH_2^+$ (**1**) through the cyclic transition structure **TS 1-2** lying 44.5 kcal mol^{-1} above **2**. Structure **1** displays a P−O bond distance of 1.899 Å and a charge (+1.139) and spin density (0.976) mostly located on the phosphorus atom. Its formation from $PF^+(^2\Pi)$ and H_2O is 48.0 kcal mol^{-1} exothermic and does not exhibit any energy barrier, as confirmed by a reaction coordinate calculation at the G2 level of theory. This exothermicity provides the system with sufficient energy to overcome all the activation barriers lying below the reactant back-dissociation limit. Among these, the O−H bond cleavage in **1** ($D°$ = 31.1 kcal mol^{-1}) produces the $FP-OH^+$ structure **7c**. The structure of $HF-P-OH^+$ (**3**) is 14.5 kcal mol^{-1} less stable than the global minimum **2**. The long F−P distance in **3** (2.142 Å) supports the view of a loosely-bound complex between HF and POH^+ (**4**), which is connected to both **1** and **2** through the corresponding cyclic transition states **TS 1-3** (32.1 kcal mol^{-1} above **1**) and **TS 2-3** (52.7 kcal mol^{-1} above **2**). Dissociation of **3** ($D°$ = 13.1 kcal mol^{-1}) yields the separated HF and POH^+ (**4**) fragments. The long F−P distance in the high-energy $HF-PH-O^+$ critical structure (**5**) (2.087 Å)

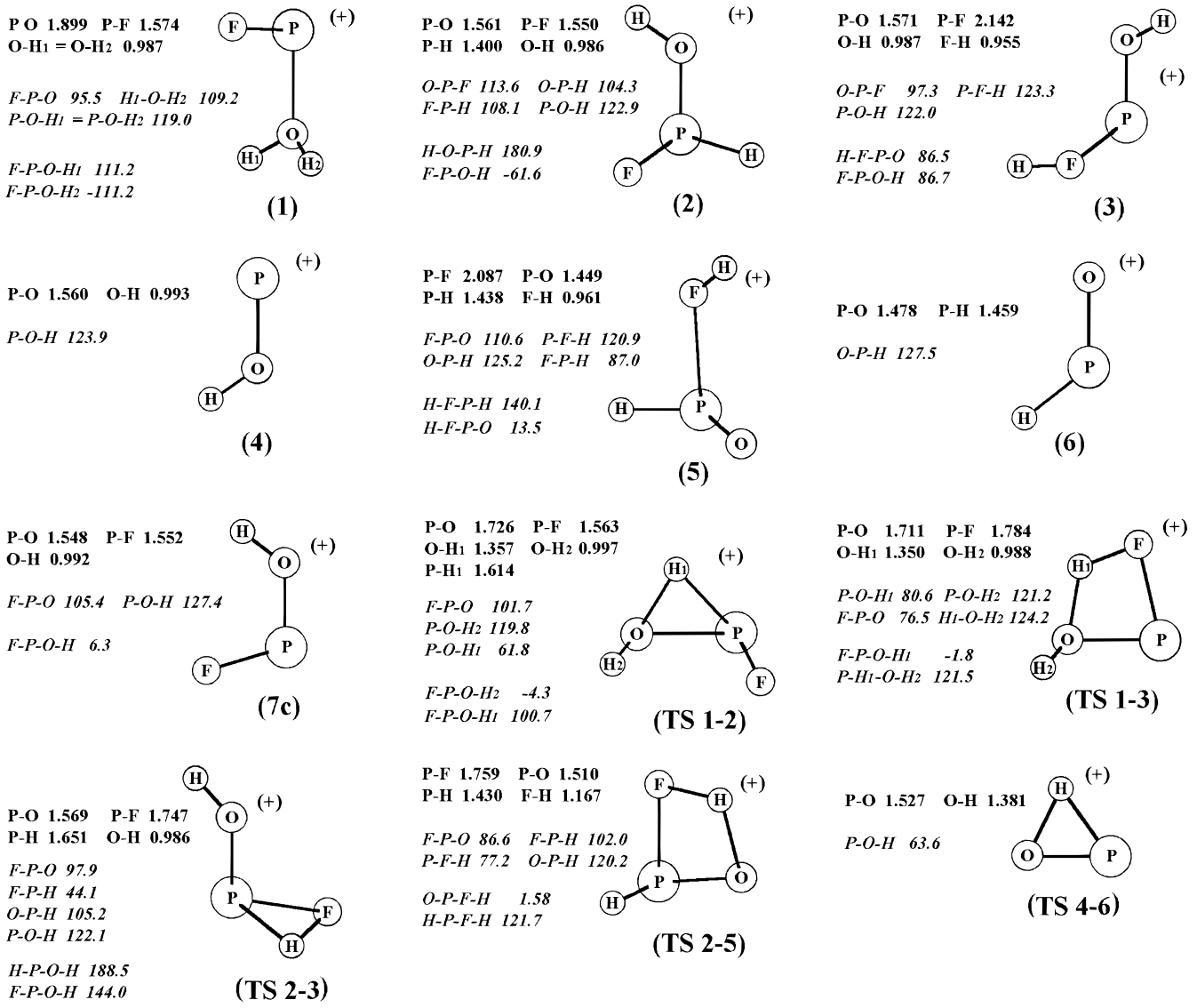

Figure 2. MP2(FULL)/6-31G* optimized geometries of the $[PF, H_2O]^+$ critical structures; bond lengths in angstroms (boldface notations) and bond angles in degrees (italic notations).

Table 3. G2 Total Energies, Enthalpies, and Free Energies (au) of the Species Involved in the Doublet $[PF, H_2O]^+$ PES

species		NIMAG[a] (cm^{-1})	E_0	H_{298}	G_{298}	$\langle S^2 \rangle$	ΔE_0 (kcal mol^{-1})	ΔG_{298} (kcal mol^{-1})
$PF^+(^2\Pi)$		0	−440.266 32	−440.262 98	−440.287 98	0.7500		
H_2O		0	−76.332 05	−76.328 27	−76.349 65		0.0	0.0
1		0	−516.674 82	−516.669 07	−516.702 77	0.7501	−48.0	−40.8
2		0	−516.680 53	−516.675 69	−516.707 03	0.7500	−51.6	−43.5
3		0	−516.657 48	−516.651 18	−516.686 12	0.7501	−37.1	−30.4
$POH^+(^2A')$	**4**	0	−416.286 58	−416.282 69	−416.309 66	0.7501		
HF		0	−100.350 01	−100.346 70	−100.366 39		−24.0	−24.1
5		0	−516.618 51	−516.612 48	−516.646 69	0.7506	−12.7	−5.7
$HPO^+(^2A')$	**6**	0	−416.240 80	−416.236 90	−416.264 43	0.7534		
HF		0	−100.350 01	−100.346 70	−100.366 39		+4.7	+4.3
$FPOH^+(^1A')$	**7c**	0	−516.125 24	−516.120 80	−516.150 72			
H		0	−0.500 00	−0.497 64	−0.510 65		−16.9	−14.9
TS 1-2		1 (2032i)	−516.604 58	−516.604 88	−516.636 11	0.7520	−7.1	+0.9
TS 1-3		1 (1727i)	−516.623 63	−516.619 08	−516.650 09	0.7501	−15.9	−7.8
TS 2-3		1 (1846i)	−516.596 63	−516.591 53	−516.623 48	0.7512	+1.1	+8.9
TS 2-5		1 (1871i)	−516.585 49	−516.581 07	−516.611 84	0.7504	+8.1	+16.2
TS 4-6		1 (2399i)	−416.213 40	−416.209 59	−416.236 85	0.7536		
HF		0	−100.350 01	−100.346 70	−100.366 39		+21.9	+21.6

[a] Number of imaginary frequencies.

is consistent with a loosely-bound complex between HF and HPO^+ (**6**). Structure **5** is connected to the 38.9 kcal mol^{-1} more stable isomer **2** through the cyclic transition state **TS 2-5**, whose energy protrudes 8.1 kcal mol^{-1} above the back-dissociation limit. Cleavage of the F−P interaction in **5** ($D° = 17.4$ kcal mol^{-1}) yields the separated HF and HPO^+ (**6**) fragments.

As a whole, most of the minima of the $[PF, H_2O]^+$ PES, i.e. **1**−**3** and **5**, and some of the transition structures involved

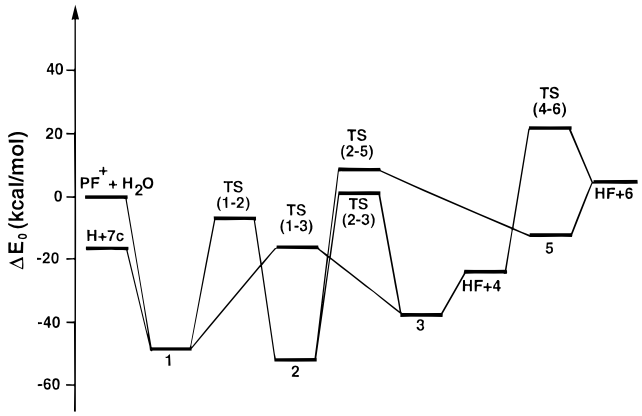

Figure 3. Two-dimensional GAUSSIAN-2 potential energy diagram of the $[PF, H_2O]^+$ species. Notations are as in Table 3 and Figure 2.

in their interconversion, i.e. **TS 1-2** and **TS 1-3**, are situated below the energy level of the reactants. However, according to the G2-calculated G_{298} values of Table 3, the stepwise process **1** → **2** → **3** involves activation free energies at 298 K protruding above the reactant limit (0.9 and 8.9 kcal mol^{-1}). Therefore, only two major reaction channels are kinetically accessible to the $PF^+(^2\Pi) + H_2O$ system, i.e. $PF^+(^2\Pi) + H_2O \rightarrow$ **1** → H + $FP{-}OH^+(^1A')$ ($\Delta H_{298} = -17.1$ kcal mol^{-1}) and $PF^+(^2\Pi) + H_2O \rightarrow$ **1** → **TS 1-3** → **3** → HF + $POH^+(^2A')$ ($\Delta H_{298} = -23.9$ kcal mol^{-1}), as confirmed by the FT-ICR experiments (Table 1). Yet the major efficiency of the latter pathway, relative to the first one (Table 1), does not conform to the relevant computed free energy barriers at 298 K, i.e. 33.0 and 25.9 kcal mol^{-1}, respectively (Table 3). Formation of the free HPO^+ product **6** from the $PF^+(^2\Pi) + H_2O$ reaction is expected to be prevented by both thermodynamic ($\Delta G_{298} = +4.3$ kcal mol^{-1}; $\Delta H_{298} = +4.8$ kcal mol^{-1}; Table 3) and kinetic factors, owing to the exceedingly high activation barriers (+16.2 (**TS 2-5**) and +21.6 kcal mol^{-1} (**TS 4-6**) above the reactant limit; Table 3) involved in the pathways leading to its precursor **5**. Incidentally, it should be noted that, by combining the computed 298 K enthalpy changes of $PF^+(^2\Pi) + H_2O \rightarrow$ HF + $POH^+(^2A')$ ($\Delta H_{298} = -23.9$ kcal mol^{-1}) and $PF^+(^2\Pi) + H_2O \rightarrow$ HF + $HPO^+(^2A')$ ($\Delta H_{298} = +4.8$ kcal mol^{-1}) with the experimental heats of formation of H_2O ($\Delta H_{298} = -57.8$ kcal mol^{-1}) and HF ($\Delta H_{298} = -65.1$ kcal mol^{-1}) and with the theoretical heats of formation of $POH^+(^2A')$ ($\Delta H_{298} = 196.9$ kcal mol^{-1}) and $HPO^+(^2A')$ ($\Delta H_{298} = 224.5$ kcal mol^{-1}),[11d] we estimate a *theoretical* enthalpy of formation for the $PF^+(^2\Pi)$ ion that ranges between 212.4 and 213.5 kcal mol^{-1}, in good agreement with the highest limiting value of 212 kcal mol^{-1} derived from photoionization mass spectrometric experiments.[20a]

Concerning the $[PF, NH_3]^+$ PES, several critical structures have been located along the reaction coordinate which connects the $PF^+(^2\Pi)$ and NH_3 reactants to their products. Their MP2-(FULL)/6-31G* optimized geometries are shown in Figure 4. The relevant data for the evaluation of the corresponding G2 energies are given in Table 4. The two-dimensional $[PF, NH_3]^+$ PES is shown schematically in Figure 5.

The structure of $FP{-}NH_3^+$ (**8**) represents the global minimum. It is connected to the 18.4 kcal mol^{-1} less stable protomer $F{-}PH{-}NH_2^+$ (**9**) through the cyclic transition state **TS 8-9**, which lies 51.5 kcal mol^{-1} above **8** (Figure 4). Structure **8** displays a P−N bond distance of 1.912 Å and a charge (+1.036) and spin density (0.985) mostly located on the phosphorus atom. Its formation from $PF^+(^2\Pi) + NH_3$ is too exothermic (78.1 kcal mol^{-1}) to exhibit any activation barrier, as confirmed by a reaction coordinate calculation at the G2 level of theory. This exceedingly high exothermicity imparts to the system the excess energy necessary to overcome all the activation barriers along the reaction coordinate lying below the reactants' limit. Among these, the N−H bond dissociation in **8** ($D° = 48.6$ kcal mol^{-1}) yields the $FP{-}NH_2^+$ structure (**14**). The structure of $HF{-}P{-}NH_2^+$ (**10**) is 25.0 kcal mol^{-1} less stable than the global minimum **8**. The exceedingly long F−P distance in **10** (2.377 Å) points to a loosely-bound complex between HF and PNH_2^+ (**11**), which is connected to both **8** and **9** through the corresponding cyclic transition states **TS 8-10** (48.7 kcal mol^{-1} above **8**) and **TS 9-10** (26.5 kcal mol^{-1} above **9**). Cleavage of the weak interaction in **10** ($D° = 8.7$ kcal mol^{-1}) yields the separated HF and PNH_2^+ (**11**) fragments. The long F−P distance in the least stable $HF{-}PH{-}NH^+$ protomer (**12**) (2.299 Å) is consistent with a loosely-bound complex between HF and $HPNH^+$ (**13**). Structure **12** is 55.4 kcal mol^{-1} less stable than the global-minimum isomer **8.** It is separated from structure **9** by an exceedingly high energy barrier (**TS 9-12**; 62.2 kcal mol^{-1} above **9**). Cleavage of the weak interaction in **12** ($D° = 8.9$ kcal mol^{-1}) yields the separated HF and $HPNH^+$ (**13**) fragments.

In conclusion, all the minima of the $[PF, NH_3]^+$ PES, i.e. **8**−**10** and **12**, and some of the transition structures involved in their prototropic rearrangement, i.e. **TS 8-9**, **TS 8-10**, and **TS 9-10**, are situated much lower in energy than the reactants. According to the G2-calculated G_{298} values of Table 4,

Table 4. G2 Total Energies, Enthalpies, and Free Energies (au) of the Species Involved in the Doublet $[PF, NH_3]^+$ PES

species		NIMAG[a] (cm^{-1})	E_0	H_{298}	G_{298}	$\langle S^2 \rangle$	ΔE_0 (kcal mol^{-1})	ΔG_{298} (kcal mol^{-1})
$PF^+(^2\Pi)$		0	−440.266 32	−440.262 98	−440.287 98	0.7500	0.0	0.0
NH_3		0	−56.458 67	−56.454 86	−56.477 70			
8		0	−496.840 49	−496.835 58	−496.868 44	0.7501	−78.1	−64.5
9		0	−496.820 12	−496.814 86	−496.847 09	0.7501	−59.7	−51.1
10		0	−496.809 55	−496.802 61	−496.839 20	0.7506	−53.1	−46.1
$PNH_2^+(^2B_2)$	**11**	0	−396.445 68	−396.441 72	−396.468 65	0.7517	−44.4	−43.5
HF		0	−100.350 01	−100.346 70	−100.366 39			
12		0	−496.761 22	−496.754 10	−496.790 80	0.7510	−22.7	−15.8
$HPNH^+(^2A')$	**13**	0	−396.396 99	−396.392 65	−396.420 90	0.7599	−13.8	−13.6
HF		0	−100.350 01	−100.346 70	−100.366 39			
$FPNH_2^+(^1A')$	**14**	0	−496.271 99	−496.267 47	−496.297 55		−29.5	−26.7
H		0	−0.500 00	−0.497 64	−0.510 65			
TS 8-9		1 (2287i)	−496.767 33	−496.762 44	−496.793 99	0.7527	−26.6	−17.8
TS 8-10		1 (1504i)	−496.771 86	−496.767 23	−496.798 44	0.7501	−29.4	−20.6
TS 9-10		1 (531i)	−496.777 98	−496.772 33	−496.805 29	0.7510	−33.2	−24.9
TS 9-12		1 (1585i)	−496.721 03	−496.716 33	−496.747 56	0.7504	+2.5	+11.4
TS 11-13		1 (2686i)	−396.359 17	−396.354 95	−396.382 92	0.7614	+10.1	+10.3
HF		0	−100.350 01	−100.346 70	−100.366 39			

[a] Number of imaginary frequencies.

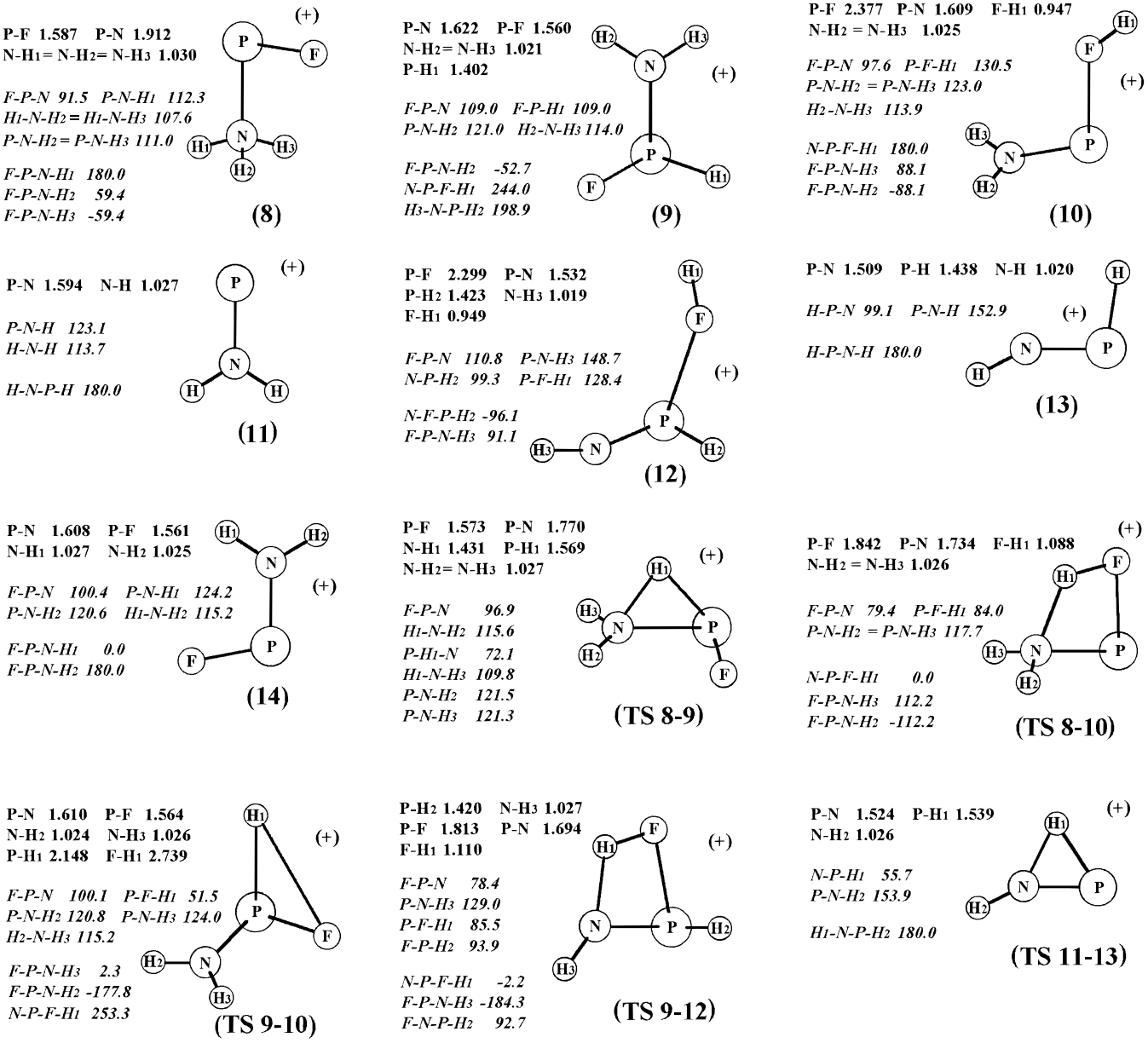

Figure 4. MP2(FULL)/6-31G* optimized geometries of the [PF, NH_3]$^+$ critical structures; bond lengths in angstroms (boldface notations) and bond angles in degrees (italic notations).

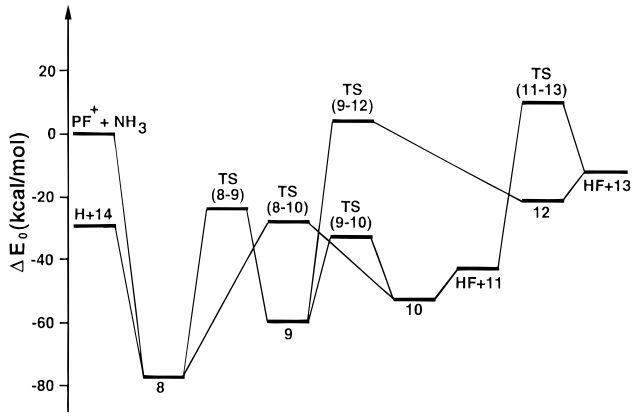

Figure 5. Two-dimensional GAUSSIAN-2 potential energy diagram of the [PF, NH_3]$^+$ species. Notations are as in Table 4 and Figure 4.

interconversions among protomers **8**−**10** involve activation free energies at 298 K lying at least ca. 17 kcal mol^{-1} below the reactant back-dissociation limit and, therefore, are all kinetically allowed. On the contrary, the free energy activation barrier for the interconversion between **9** and **12** protrudes ca. 11 kcal mol^{-1} above the reactant limit. For this reason, formation of the HF + $HPNH^+(^2A')$ (**13**) products from the $PF^+(^2\Pi)$ + NH_3 reaction, although thermodynamically allowed ($\Delta G_{298} = -13.6$ kcal mol^{-1}; Table 4), is kinetically prevented. Thus, only two reaction channels are open to the $PF^+(^2\Pi)$ + NH_3 system, namely $PF^+(^2\Pi)$ + NH_3 → **8** → H + FP−NH_2^+ ($^1A'$) and $PF^+(^2\Pi)$ + NH_3 → **8** → **10** → HF + $PNH_2^+(^2B_2)$. The accuracy of the theoretical approach used (±2 kcal mol^{-1}) prevents us from determining whether the **8** → **10** step of the latter process is direct or stepwise, i.e. **8** → **9** → **10** (Table 4). This picture fully agrees with the FT-ICR kinetic evidence (Table 1). The major efficiency of the $PF^+(^2\Pi)$ + NH_3 → **8** → H + FP−NH_2^+ pathway, relative to $PF^+(^2\Pi)$ + NH_3 → **8** → **TS 8-10** → **10** → HF + $PNH_2^+(^2B_2)$ (Table 1), is consistent with the relevant computed free energy barriers at 298 K, i.e. 37.8 and 43.9 kcal mol^{-1}, respectively (Table 4).

Combining the computed 298 K enthalpy changes of $PF^+(^2\Pi)$ + NH_3 → HF + $PNH_2^+(^2B_2)$ ($\Delta H_{298} = -44.3$ kcal mol^{-1}) and $PF^+(^2\Pi)$ + NH_3 → HF + $HPNH^+(^2A')$ ($\Delta H_{298} = -13.5$

Table 5. Efficiencies of Proton Transfer from $(PO)H^+$ to Neutral Substrates

substrate	PA (kcal mol^{-1})	IE (kcal mol^{-1})	k_{H^+}[a] (10^{10} cm^3 molecule^{-1} s^{-1})	k_{coll}[b] (10^{10} cm^3 molecule^{-1} s^{-1})	protonation efficiency
(a) CH_3Cl	155.5	258.7	nd	20.9	<0.001
(b) CH_3Br	158.3	243.1	nd	23.1	<0.001
(c) PF_3	162.5	264	nd	12.3	<0.001
(d) C_2H_4	162.6	242.3	nd	11.5	<0.001
(e) H_2O	165.0	250.8	2.8	24.7	0.11
(f) CF_3CH_2OH	167.2	265.0	7.4	11.0	0.67
(g) H_2S	168.7	240.9	10.2	14.8	0.69

[a] Uncertainty range: ca. 20%, nd < 0.01. [b] Estimated according to the trajectory calculation method.[21]

Table 6. Efficiencies of Proton Transfer from $(FPO)H^+$ to Neutral Substrates

substrate	PA (kcal mol^{-1})	IE (kcal mol^{-1})	k_{H^+}[a] (10^{10} cm^3 molecule^{-1} s^{-1})	k_{coll}[b] (10^{10} cm^3 molecule^{-1} s^{-1})	protonation efficiency
(b) CH_3Br	158.3	243.1	nd	16.7	<0.001
(c) PF_3	162.5	264	nd	11.1	<0.001
(d) C_2H_4	162.6	242.3	nd	10.9	<0.001
(e) H_2O	165.0	250.8	2.9	23.7	0.12
(f) CF_3CH_2OH	167.2	265.0	8.2	9.8	0.84
(g) H_2S	168.7	240.9	11.4	13.9	0.82
(h) CH_3OH	181.7	250.2	16.8	19.8	0.85

[a] Uncertainty range ca. 20%; nd < 0.01. [b] Estimated according to the trajectory calculation method.[21]

Table 7. Efficiencies of Proton Transfer from $(PNH)H^+$ to Neutral Substrates

substrate	PA (kcal mol^{-1})	IE (kcal mol^{-1})	k_{H^+}[a] (10^{10} cm^3 molecule^{-1} s^{-1})	k_{coll}[b] (10^{10} cm^3 molecule^{-1} s^{-1})	protonation efficiency
(b) CH_3Br	158.3	243.1	nd	18.7	<0.001
(c) PF_3	162.5	264	nd	12.4	<0.001
(d) C_2H_4	162.6	242.3	nd	11.5	<0.001
(e) H_2O	165.0	250.8	0.5	24.8	0.02
(h) CH_3CN	188.2	281.2	0.4	39.1	0.01
(i) *i*-C_3H_7CN	193.2	260.6	1.9	37.6	0.05
(j) CH_3COOCH_3	195.0	237.0	6.8	19.5	0.35
(k) $CH_3COOC_2H_5$	198.1	231.1	10.9	20.1	0.54
(l) (*n*-$C_4H_9)_2O$	203.7	217	13.3	19.1	0.70

[a] Uncertainty range ca. 20%; nd < 0.01. [b] Estimated according to the trajectory calculation method.[21]

kcal mol^{-1}) with the experimental heats of formation of NH_3 ($\Delta H_{298} = -11.0$ kcal mol^{-1}), HF ($\Delta H_{298} = -65.1$ kcal mol^{-1}), and $PF^+(^2\Pi)$ ($\Delta H_{298} = -212$ kcal mol^{-1}),[20a] we obtain *theoretical* formation enthalpies of $PNH_2^+(^2B_2)$ ($\Delta H_{298} = 221.8$ kcal mol^{-1}) and $HPNH^+(^2A')$ ($\Delta H_{298} = 252.6$ kcal mol^{-1}) which agree well with those derived for the same ions, i.e. 222.8 and 253.5 kcal mol^{-1}, respectively, from independent G2 calculations.[11a]

Proton Affinities. An experimental confirmation of the actual structure and multiplicity of the ionic products $(PO)H^+$, $(FPO)H^+$, $(PNH)H^+$, and $(FPNH)H^+$, arising from paths i and ii of Scheme 1 and paths xi and xii of Scheme 3, is sought in the comparison between their G2 calculated and the experimental standard proton loss enthalpies (H_{298}). The well-established bracketing technique is used for this purpose, which is based on the measurement of the efficiency of the proton transfer of the ion (e.g. $(PO)H^+$) to a gaseous reference base B of appropriate strength. For systems allowing exclusively or predominantly the proton transfer process, a high proton transfer efficiency is taken as an indication that the PA of B exceeds that of the conjugate base of the ion (i.e., PA(B) > PA(PO)), whereas a negligible proton transfer efficiency is taken as evidence that the PA of the conjugate base of the ion exceeds that of B (i.e., PA(B) < PA(PO)). Strictly speaking, the latter inference is not rigorous, because a proton transfer inefficiency could reflect the operation of kinetic, rather than thermodynamic, factors. This, however, seems unlikely in this case since only n-type bases were employed. In fact, exothermic proton transfer reactions involving sterically unhindered n-type bases are known to proceed at, or nearly at, the collision rate.[25] The results of the bracketing experiments are listed in Tables 5−8.

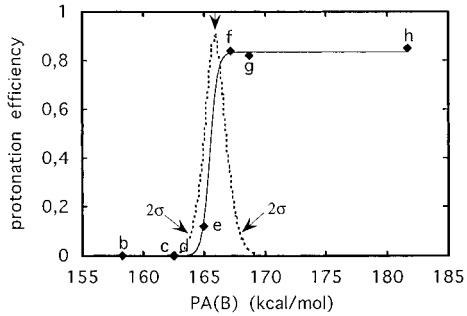

Figure 6. Efficiency of proton transfer by $(FPO)H^+$ as a function of the proton affinity (PA) of neutral bases. Lettering is as in Table 6. The first derivative of the sigmoid interpolating function is reported as the broken Gaussian curve, whose maximum is taken as the standard protonation enthalpy of $(FPO)H^+$ (see text and footnote 26).

If plotted against PA(B)'s, the proton transfer efficiency values of Tables 5−8 can be interpolated by sigmoid curves, one example of which is given in Figure 6.

The inflection of the sigmoid curves corresponds to a PA(B) value taken as equal to the PA of the conjugate base of the ion of interest. It is determined from the PA(B) value corresponding to the maximum of the first derivative of the

(25) The proton transfer efficiency may be low if the reaction is nearly thermoneutral and if it involves hindered bases. Cf.: Bucker, H.; Grutzmacher, H. F. *Int. J. Mass Spectrom. Ion Processes* **1991**, *109*, 95.

Table 8. Efficiencies of Proton Transfer from $(PNH)H^+$ to Neutral Substrates

substrate	PA (kcal mol^{-1})	IE (kcal mol^{-1})	k_{H^+}[a] (10^{10} cm^3 molecule^{-1} s^{-1})	k_{coll}[b] (10^{10} cm^3 molecule^{-1} s^{-1})	protonation efficiency
(b) CH_3Br	158.3	243.1	nd	16.8	<0.001
(c) PF_3	162.5	264	nd	11.2	<0.001
(d) C_2H_4	162.6	242.3	nd	10.9	<0.001
(e) H_2O	165.0	250.8	nd	23.8	<0.001
(g) H_2S	168.7	240.9	0.2	14.0	0.01
(m) $CH_2(CN)_2$	175.6	292.5	0.6	29.6	0.02
(h) CH_3CN	188.2	281.2	0.7	36.3	0.02
(n) $HCOOC_2H_5$	193.1	244.7	2.4	19.1	0.12
(i) i-C_3H_7CN	193.2	260.6	3.7	34.2	0.11
(j) CH_3COOCH_3	195.0	237.0	4.1	17.7	0.23
(k) $CH_3COOC_2H_5$	198.1	230.8	10.7	18.1	0.59
(m) t-$C_4H_9OCH_3$	202.2	213.1	9.0	16.0	0.56
(l) (n-C_4H_9)$_2$O	203.7	217	10.8	17.0	0.63

[a] Uncertainty range ca. 20%; nd < 0.01. [b] Estimated according to the trajectory calculation method.[21]

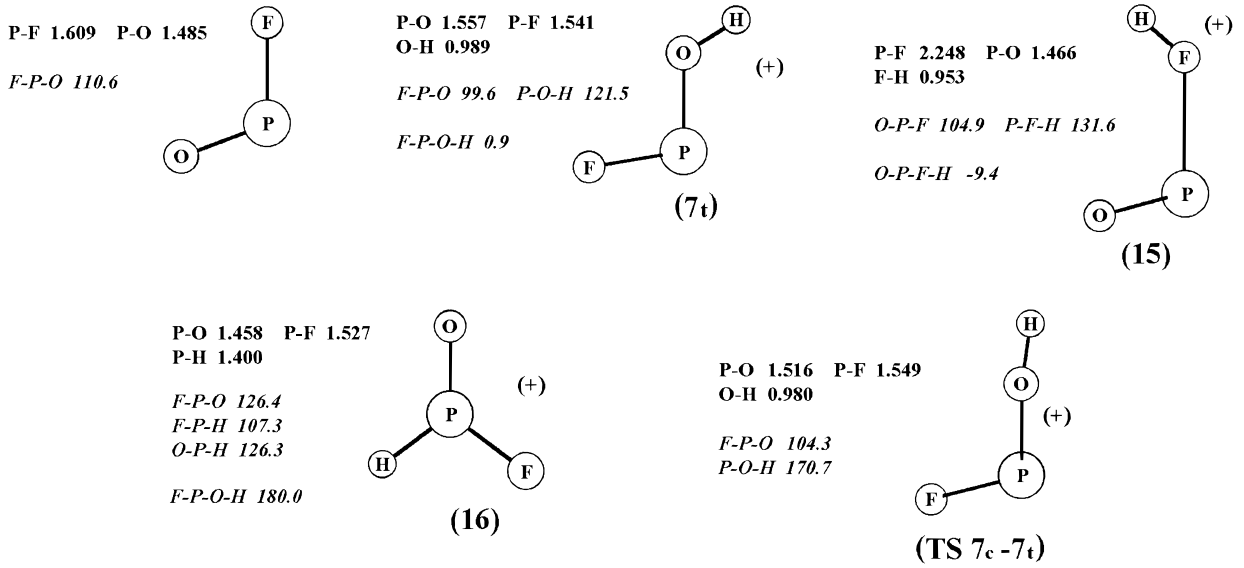

Figure 7. MP2(FULL)/6-31G* optimized geometries of the FPO molecule and the $(FPO)H^+$ species; bond lengths in angstroms (boldface notations) and bond angles in degrees (italic notations).

function expressing the sigmoid curves. The uncertainties of the PA measurements are taken as equal to the 2σ parameter of the normal Gaussian distribution of the derivative function.[26] The proton loss enthalpies obtained by this procedure for the $(PO)H^+$, $(FPO)H^+$, $(PNH)H^+$, and $(FPNH)H^+$ ions are compared with the relevant G2 protonation energies of their conjugate bases, calculated at 298 K (H_{298}).

The G2-calculated protonation energies of the various [H, O, P]$^+$ and [H_2, N, P]$^+$ isomers are known from the literature.[11a,b] Ab initio quantum mechanical calculations of the protonation of FPO(^{1}A′) and FP−NH(^{1}A′) have been addressed in the present study. The existence and the relative stability of the various isomers from protonation at the oxygen, phosphorus, and fluorine of FPO(^{1}A′) and at the nitrogen, phosphorus, and fluorine of FP−NH(^{1}A′) have been examined at the G2 level of theory.

Positive evidence for the existence of four $(FPO)H^+$ distinct isomers has been obtained. Their optimized geometries, at the MP2(FULL)/6-31G* level, are reported in Figure 7, together with that of the FPO(^{1}A′) molecule. Analysis of Figure 7 provides further support for the rule proposed by Alcami et al.[27] regarding the structural distortion of species with different basic centers when undergoing protonation. Accordingly, protonation at the most electronegative F and O centers of FPO(^{1}A′) leads to a weakening and a lengthening of the bond in which the basic center participates, i.e. the F−P of **15** and the P−O bond of **7**, respectively, whereas protonation at the less electronegative P atom leads to a reinforcement of the linkages in which the center participates, i.e. both the F−P and the P−O bonds of **16**. In the first case, lengthening of the F−P or the P−O bond is also accompanied by a decrease of the F−P−O bond angle, whereas, in the latter case, shortening of the same bonds is accompanied by an increase of the same angle. These observations point to a legitimate extension of the rule of Alcami to bases containing second-row elements.

The G2 energies of the species in Figure 7 are reported in Table 9. Protonation at the oxygen atom of FPO(^{1}A′) gives the stable cis **7c** (Figure 2) and trans **7t** isomers, the former being more stable by 1.2 kcal mol^{-1} at the G2 level of theory. Interconversion between **7c** and **7t** occurs through the transition structure **TS 7c−7t**, which lies only 4.4 kcal mol^{-1} above **7c**. The fluorine-protonated isomer **15** and the phosphorus-protonated planar structure **16** were found to be less stable than **7c** by 21.9 and 35.5 kcal mol^{-1}, respectively. According to Table 9, the G2-calculated PA ($=-\Delta H_{298}$) at the oxygen atom of FPO(^{1}A′), assuming the formation of **7c**, is estimated as 165.9 kcal mol^{-1} and that at its fluorine atom as 143.1 kcal mol^{-1} whereas

(26) The 2σ parameter is taken just to characterize the normal Gaussian distribution of the derivative function, since the distribution itself and, therefore, the 2σ parameter do not have any statistical significance.

(27) Alcami, M.; Mò, O.; Yanez, M.; Abboud, J. L. M.; Elguero, J. *Chem. Phys. Lett.* **1990**, *172*, 471.

Table 9. G2 Total Energies, Enthalpies, and Free Energies (au) of Singlet F−P−O and (F−P−O)H^+

species	NIMAG[a] (cm^{-1})	E_0	H_{298}	G_{298}	ΔH_{298} (kcal mol^{-1})
F−P−O	0	−515.863 00	−515.858 85	−515.888 21	0.0
cis-F−P−OH^+ (**7c**)	0	−516.125 24	−516.120 80	−516.150 72	−165.9
trans-F−P−OH^+ (**7t**)	0	−516.123 37	−516.118 95	−516.148 79	−164.7
HF−PO^+ (**15**)	0	−516.674 82	−516.669 07	−516.702 77	−143.1
F−PH−O^+ (**16**)	0	−516.068 72	−516.064 40	−516.093 98	−130.5
TS 7c−7t	1 (654i)	−516.118 29	−516.113 64	−516.143 98	−161.4

[a] Number of imaginary frequencies.

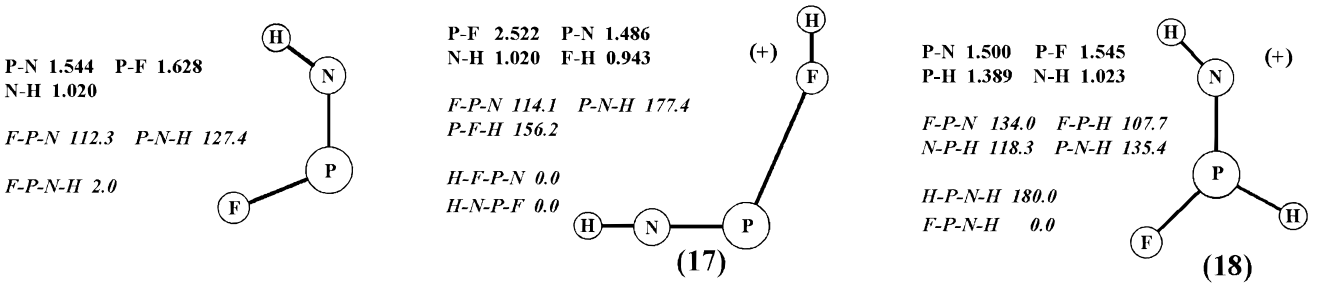

Figure 8. MP2(FULL)/6-31G* optimized geometries of the FP−NH molecule and the (FP−NH)H^+ species; bond lengths in angstroms (boldface notations) and bond angles in degrees (italic notations).

Table 10. G2 Total Energies, Enthalpies, and Free Energies (au) of Singlet F−P−NH and (F−P−NH)H^+

species	NIMAG[a]	E_0	H_{298}	G_{298}	ΔH_{298} (kcal mol^{-1})
F−P−NH	0	−495.963 48	−495.959 04	−495.988 91	0.0
F−P−NH_2^+ (**14**)	0	−496.271 99	−496.267 47	−496.297 55	−195.0
HF−P−NH^+ (**17**)	0	−496.233 19	−496.226 38	−496.262 42	−169.2
F−PH-NH^+ (**18**)	0	−496.204 36	−496.199 63	−496.229 86	−152.4

[a] Number of imaginary frequencies.

that at its phosphorus atom is estimated as 130.5 kcal mol^{-1} at 298 K.

Protonation of FP−NH($^1A'$) provides three distinct stable isomers, whose optimized geometries, at the MP2(FULL)/6-31G* level, are reported in Figure 8, together with that of the FP−NH($^1A'$) molecule. Again, analysis of Figure 8 indicates that protonation at its different basic centers modifies the bond lengths and angles of the FP−NH($^1A'$) species in agreement with the rule of Alcami.[27]

The G2 energies of the species in Figure 8 are listed in Table 10. Protonation at the nitrogen atom of FP−NH($^1A'$) gives the stable planar structure **14** (Figure 4). At the G2 level of theory, the fluorine-protonated isomer **17** and the phosphorus-protonated planar structure **18** were found to be less stable than **14** by 24.3 and 42.4 kcal mol^{-1}, respectively. According to Table 10, the PA at the nitrogen atom of FP−NH($^1A'$) is computed at the G2 level of theory to be 195.0 kcal mol^{-1} and that at its fluorine atom is estimated as 169.2 kcal mol^{-1} whereas that at its phosphorus atom is 152.4 kcal mol^{-1} at 298 K.

The G2-calculated PA's at the different centers of PO($^2\Pi$), FPO($^1A'$), PNH($^2A'$), HPN($^2A'$), and FP−NH($^1A'$) are compared in Table 11 with the relevant experimental values obtained from the FT-ICR bracketing experiments.

Coincidence among the experimental proton loss enthalpies of the (PO)H^+, (FPO)H^+, and (FP−NH)H^+ fragments from the reaction sequences of Schemes 1−6 and the G2-calculated PA's of the oxygen of PO($^2\Pi$) and FPO($^1A'$) and of the nitrogen of FP−NH($^1A'$) provides unequivocal evidence regarding their actual structure and multiplicity, i.e. POH^+($^2A'$), $FPOH^+$($^1A'$), and FP−NH_2^+ ($^1A'$), respectively. Instead, the measured proton loss enthalpy of (PNH)H^+ (195.6 ± 3.3 kcal mol^{-1}) only closely approaches the 298 K G2-calculated proton affinity of the nitrogen of PNH($^2A_1$) (201.0 ± 2 kcal mol^{-1}).[11a] Nevertheless, taking into account the much larger differences between the experimental (PNH)H^+ proton loss enthalpy and those computed

Table 11. Experimental and Calculated Proton Affinities (kcal mol^{-1}) of P−O($^2\Pi$), F−P−O($^1A'$), P−N−H($^2A'$), H−P−N($^2A'$), and F−P−NH($^1A'$)

	PA_{theor}	PA_{exp}
P−O($^2\Pi$) + H^+ → P−O−H^+($^2A'$)	165.5[a]	165.9 ± 2.1[b]
→ H−P−O^+($^2A'$)	140.4[a]	
F−P−O($^1A'$) + H^+ → *cis*-F−P−OH^+($^1A'$)	165.9	165.9 ± 2.1
→ *trans*-F−P−OH^+($^1A'$)	164.7	
→ HF−PO^+($^1A'$)	143.1	
→ F−PH−O^+($^1A'$)	130.5	
P−N−H($^2A'$) + H^+ → P−NH_2^+($^2B_2$)	201.0[c]	195.6 ± 3.3
→ HP−NH^+($^2A'$)	170.3[c]	
H−P−N($^2A'$) + H^+ → HP−NH^+($^2A'$)	185.3[c]	
→ H_2P−N^+($^2A_1$)	90.3[c]	
F−P−NH($^1A'$) + H^+ → F−P−NH_2^+($^1A'$)	195.0	194.3 ± 2.1
→ HF−P−NH^+($^1A'$)	169.2	
→ F−PH−NH^+($^1A'$)	152.4	

[a] Reference 11b. [b] A value of 163 ± 2 kcal mol^{-1} is quoted in ref 4d. [c] Derived using $H°_f(H^+)$ = 365.7 kcal mol^{-1} and standard formation enthalpies of the phosphorus species as estimated in ref 11a.

for the other $[H_2, N, P]^+$ isomers (Table 11), it can be safely concluded that the (PNH)H^+ fragment formed from the attack of PF^+($^2\Pi$) on NH_3 (path xii in Scheme 3) has the structure and the multiplicity of the stable isomer PNH_2^+($^2B_2$) (**11** in Figure 4).

Comparison with Related Ionic Species. Compared to nitrogen, phosphorus is much less electronegative (its Pauling electronegativity is close to that of hydrogen (=2.1)) and has low-energy empty d orbitals. These different electronic properties are reflected in the large difference in structure and the relative stability of the members of the corresponding (XNH)-H^+ and (FXO)H^+ (X = N, P) ion families.

The G2 global minimum of the doublet (N_2H)H^+ PES is represented by the *trans*-$HNNH^+$ structure, which is 6.2 kcal mol^{-1} more stable than the *cis*-$HNNH^+$ isomer and 3.5 kcal

mol^{-1} more stable than NNH_2^+.[28] In the corresponding doublet $(PNH)H^+$ PES, instead, the global minimum is the PNH_2^+ structure (**11**), which is 30.6 kcal mol^{-1} more stable than the *trans*-$HPNH^+$ isomer (**13**). No stable *cis*-$HPNH^+$ structure was located on the doublet $(PNH)H^+$ PES. Bond lengths and electronic charge densities reveal that both *trans*-$HNNH^+$ and *trans*-$HPNH^+$ (**13**) have similar valence electron distributions, with partial N−N and N−P triple bonding, respectively.[11a,28] Partial triple bonding is also present between the nitrogens of NNH_2^+. However, in the corresponding PNH_2^+ structure (**11**), most of the positive charge is located at the phosphorus center (+0.879), which is connected to the nitrogen atom essentially by a double bond. The lack of a critical point on the doublet $(PNH)H^+$ PES corresponding to the *cis*-$HPNH^+$ structure contrasts with the occurrence of a stable *cis*-$HNNH^+$ structure in the doublet $(N_2H)H^+$ PES and with the sizable activation barrier (11.2 kcal mol^{-1}) involved in its conversion to *trans*-$HNNH^+$.[29] Another noteworthy difference concerns the bond angles of *trans*-$HNNH^+$ and *trans*-$HPNH^+$ (**13**). In the first, the H−N−N angle is 123.5°,[28] whereas in **13** the H−P−N angle is 99.1° and the P−N−H angle is 152.9° . It is tempting to attribute the above differences to partial sp hydridization of the nitrogen atom, favored by some stabilizing interaction between its p electron(s) and the empty d orbital of the adjacent phosphorus.

Ab initio Gaussian-1 (G1) calculations point to the fluorine-protonated form $HF-NO^+$ as the global minimum among the $(FNO)H^+$ protomers,[24b,30] more stable by ca. 63 and ca. 72 kcal mol^{-1} than $FN-OH^+$ and $F-NH-O^+$, respectively. In addition, calculations demonstrate that fluorine protonation of FNO induces a decrease of both the N−O bond distance (from 1.159 to 1.103 Å) and the F−N−O angle (from 106.8 to 91.6°). This is consistent with the concept of $HF-NO^+$ as a loosely-bound complex between HF and NO^+. Although the interaction between HF and NO^+ is relatively weak ($D°$ = 14.6 kcal mol^{-1} (N−F)),[24b] the overall energy of this system is significantly lower than that of any of its protomers. The fact that the triple bond in NO^+ is one of the strongest in all of chemistry ($D°$ = 250 kcal mol^{-1})[31] is of course a major contributor to the enormous relative stability of the $HF-NO^+$ complex. Fluorine protonation of FPO involves a comparatively less pronounced structural reorganization. In FPO and its planar fluorine-protonated structure **15**, the P−O bond distances and the F−P−O angles are only slightly modified (1.485 vs 1.466 Å; 110.6 vs. 104.9°). These findings, coupled with the positive charge location at the P atom (+1.305) of $HF-PO^+$, exclude significant π-electron back-donation from oxygen to phosphorus in the PO^+ moiety. On these grounds, taking into account the comparable F−X (X = N, P) dissociation energies of $HF-NO^+$ ($D°$ = 14.6 kcal mol^{-1})[24b] and $HF-PO^+$ ($D°$ = 15.0 kcal mol^{-1}), it is suggested that the instability of the PO^+ moiety, relative to NO^+, plays a significant role in determining the minor stability of $HF-PO^+$ relative to its protomers.

The least stable structures of the $(FNO)H^+$ family are *cis*- and *trans*-$FN-OH^+$.[24b] The corresponding structures of the $(FPO)H^+$ family, i.e. *cis*- (**7c**) and *trans*-$FP-OH^+$ (**7t**), are instead the most stable isomers. This dramatic effect is also attributable to the effect of the phosphorus atom. Destabilization in *cis*- and *trans*-$FN-OH^+$ is ascribed to the relatively short N−O bond distances (1.248 Å (trans); 1.237 Å (cis)), which enhance repulsive interactions between the lone pair of oxygen and the lone pair of nitrogen or of the N−F bond electrons.

In *cis*-$FP-OH^+$ (**7c**), instead, the same destabilizing interactions are less pronounced, owing to the comparatively long P−O distance (1.548 Å) and the 6.3° flipping of the F atom away from the P−O−H plane. Compared to the 140.5° N−O−H angle of the transition structure separating *cis*- and *trans*-$FN-OH^+$, the 170.7° P−O−H angle in the transition structure **TS 7c−7t** is noteworthy. Indeed, the single imaginary frequency of **TS 7c−7t**, −621 cm^{-1}, corresponds to a quasi-in-plane rotation of the O−H bond. This observation, coupled with the small activation barrier for the interconversion between **7c** and **7t** (E_0(**TS 7c−7t**) − E_0(**7c**) = 4.4 kcal mol^{-1}), suggests that the oxygen inversion process in $FP-OH^+$ may be favored by significant overlap between the 2p lone pairs of the oxygen atom and the empty 3d orbitals of the P^+ center. The same interaction is prevented in the transition structure involved in the interconversion of *cis*- and *trans*-$FN-OH^+$, whose activation barrier amounts to over 25 kcal mol^{-1}.[24b]

Conclusions

The PF_n^+(n = 1, 2) + H_2O, CH_3OH, and NH_3 reactions represent convenient routes to phosphorus ions potentially involved in the formation of phosphorus molecules in outer space. Their kinetics, thermochemistry, and detailed mechanism are investigated by the joint application of FT-ICR mass spectrometry and G2 theoretical calculations. Exothermic PF_n^+(n = 1, 2) + H_2O, CH_3OH, and NH_3 reactions proceed through the intermediacy of several addition protomers separated by significant energy barriers before eliminating either an HF molecule or an H atom. The structures and the multiplicities of the obtained ionic products, i.e. POH^+($^2A'$), $FP-OH^+$($^1A'$), PNH_2^+($^2B_2$), and $FP-NH_2^+$ ($^1A'$), are unequivocally determined from the coincidence between FT-ICR bracketing measurements and G2 molecular orbital calculations of their standard protonation enthalpies. The same coincidence demonstrates that the performance of ab initio molecular orbital calculations at the G2 level of theory using MP2(FULL)/6-31G* geometry optimizations in describing structures and relative energies in the selected category of phosphorus-containing ions is fully adequate. The presence of low-energy empty d orbitals in the phosphorus atom, coupled with its low Pauling electronegativity, accounts for the structural features and the stability order of some of its ions, e.g. $(PNH)H^+$ and $(FPO)H^+$, which substantially differ from those of strictly related species where phosphorus is replaced by a nitrogen atom.

Acknowledgment. This work was supported by the Ministero della Ricerca Scientifica e Tecnologica (MURST). The authors express their gratitude to F. Grandinetti for his interest in this work and to R. Moscardelli for his skilled technical support.

IC961394R

(28) Pople, J. A.; Curtiss, L. A. *J. Chem. Phys.* **1991**, *95*, 4385.
(29) Goldberg, N.; Holthausen, M. C.; Hrusak, J.; Koch, W.; Schwarz, H. *Chem. Ber.* **1993**, *126*, 2735.
(30) Meredith, C.; Davy, R. D.; Schaefer, H. F., III. *J. Chem. Phys.* **1990**, *93*, 1215.
(31) Huber, K. P.; Herzberg, G. *Molecular Spectra and Molecular Structure. IV. Constants of Diatomic Molecules*; Van Nostrand Reinhold: New York, 1979.